

Graphene oxide functionalized long period grating for ultrasensitive label-free immunosensing

Chen Liu^a, Qi Cai^{a,b}, Baojian Xu^b, Weidong Zhu^c, Lin Zhang^d, Jianlong Zhao^{b,*}, Xianfeng Chen^{a,*}

^a School of Electronic Engineering, Bangor University, Bangor LL57 1UT, United Kingdom

^b State Key Laboratory of Transducer Technology, Shanghai Institute of Microsystem and Information Technology, Chinese Academy of Sciences, Shanghai 200050, China

^c Department of Applied Science and Technology, Saint Peter's University, NJ 07306, USA

^d Aston Institute of Photonic Technologies, Aston University, Birmingham B4 7ET, United Kingdom

ABSTRACT

We explore graphene oxide (GO) nanosheets functionalized dual-peak long period grating (dLPG) based biosensor for ultrasensitive label-free antibody-antigen immunosensing. The GO linking layer provides a remarkable analytical platform for bioaffinity binding interface due to its favorable combination of exceptionally high surface-to-volume ratio and excellent optical and biochemical properties. A new GO deposition technique based on chemical-bonding in conjunction with physical-adsorption was proposed to offer the advantages of a strong bonding between GO and fiber device surface and a homogeneous GO overlay with desirable stability, repeatability and durability. The surface morphology of GO overlay was characterized by Atomic force microscopy, Scanning electron microscope, and Raman spectroscopy. By depositing the GO with a thickness of 49.2 nm, the sensitivity in refractive index (RI) of dLPG was increased to 2538 nm/RIU, 200% that of non-coated dLPG, in low RI region (1.333-1.347) where bioassays and biological events were usually carried out. The IgG was covalently immobilized on GO-dLPG via EDC/NHS heterobifunctional cross-linking chemistry leaving the binding sites free for target analyte recognition. The performance of immunosensing was evaluated by monitoring the kinetic bioaffinity binding between IgG and specific anti-IgG in real-time. The GO-dLPG based biosensor demonstrates an ultrahigh sensitivity with limit of detection of 7 ng/mL, which is 10-fold better than non-coated dLPG biosensor and 100-fold greater than LPG-based immunosensor. Moreover, the reusability of GO-dLPG biosensor has been facilitated by a simple regeneration procedure based on stripping off bound anti-IgG treatment. The proposed ultrasensitive biosensor can be further adapted as biophotonic platform opening up the potential for food safety, environmental monitoring, clinical diagnostics and medical applications.

Keywords: Graphene oxide; Biosensor; Antibody-antigen; Long period grating; Label-free; Immunosensor

1. Introduction

The development of biosensor is extremely important for the healthcare, clinical analysis, drug discovery, and environmental and security sectors (Marks et al., 2007; Estevez et al., 2014). To overcome the drawback of traditional biosensor which is usually time consuming, complicated, labeling required and hazardous, fiber optic sensing technology has been proposed by employing fiber Bragg gratings (FBGs), long period gratings (LPGs), and tilted fiber gratings (TFGs) with the advantages of label-free, real-time, multiplex and in-line determination (Wang and Wolfbeis, 2013; James and Tatam, 2003; Albert et al., 2013; Cusano et al., 2014; Zhou et al., 2004). However, the major challenge in fiber sensor field is the lack of sensitivity for applications with small biomolecules and low concentration of

analyte (Fan and White, 2011; Canning, 2009). To improve the biosensing performance, techniques have been developed to accelerate the device sensitivity, for instance by cladding etching, side polishing and fiber tapering (Chen et al., 2005; Jang et al., 2009; Zhao et al., 2004; Ding et al., 2005). Instead of sacrificing of mechanical integrity, more elegant approaches have been investigated either by novel design of grating structures or by the deposition of thin overlay. The dual-peak LPG (dLPG) operating near the dispersion turning point owns intrinsic high sensitivity to the change of surrounding-medium refractive index (SRI) (Shu et al., 2002; Chen et al., 2007). The coating of thin film induces strong changes on the LPG transmission properties (Marques et al., 2016; Villar et al., 2005; Cusano et al., 2005; Pilla et al., 2012). Various fiber optic biosensors have been produced for the detection of protein (Lepinay et al., 2014), bioaffinity of antibody-antigen (Chiavaioli et al., 2014; DeLisa et al., 2000; He et al., 2011), DNA hybridization (Chen et al., 2007; Yin et al., 2013), cellular behavior (Shevchenko et al., 2014), enzyme-glucose binding (Deep et al., 2012; Luo et al., 2014), biotin-streptavidin (Voisin

* Corresponding authors. Tel: +44 1248 382480; fax: +44 1248 361429.
 Email address: x.chen@bangor.ac.uk (X. Chen), jlzhao@mail.sim.ac.cn (J. Zhao).

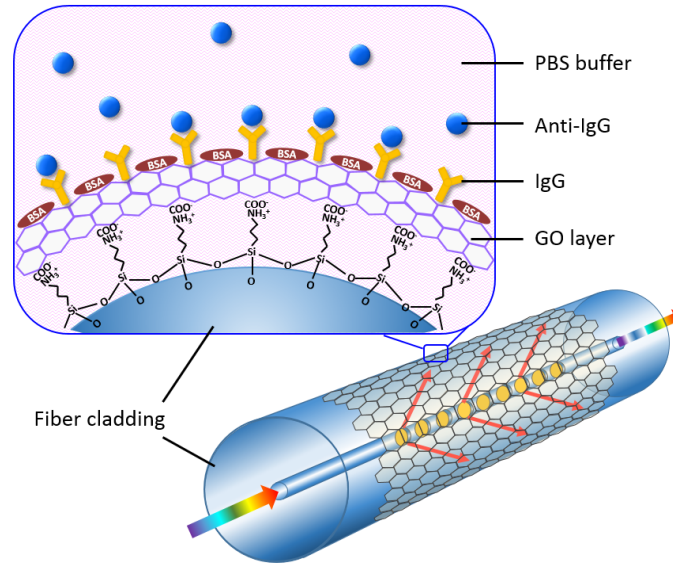


Fig. 1. Schematic diagram of fiber optic biosensor comprising the dLPG coated with the graphene oxide linking layer, which provides a remarkable analytical platform for bioaffinity binding between pre-immobilized IgG and target anti-IgG.

et al., 2014) and bacteria (Brzozowska et al., 2015).

To date, the advancement of nanotechnology plays an essential role in the exploration of multidisciplinary fields including physics, chemistry, materials, medicine and biotechnology. Biosensing benefited by nanotechnology is based on advanced materials and nanostructures as transducer elements or reporters. Graphene has attracted great excitement since its discovery (Novoselov et al, 2004; Geim, 2009). The extraordinary mechanical, electrical, chemical and optical properties make graphene a very promising carbon-based nanomaterial for widespread applications such as field-effect transistor, ultracapacitor, energy storage, sensor and ultrafast laser (Zhou et al., 2017; Bonaccorso et al., 2014, Bao et al., 2009; Bao et al., 2010). Moreover, graphene oxide (GO) displays advantageous characteristics for biosensing due to its excellent capabilities in biocompatibility, solubility and selectivity (Morales-Narvez et al., 2012; Wang et al., 2011; Loh et al., 2010). GO contains both sp^2 - and sp^3 - hybridized carbon atoms as well as different oxygen-containing functional groups such as hydroxyl, epoxy, carboxyl on its basal plane and sheet edges, which can be used for immobilization of biomolecules (Dreyer et al., 2010; Chen et al., 2012). The enriched functional groups can interact in an ionic, covalent or non-covalent manner, so that in principle they provide the highest extraction efficiency of biomolecules per unit area (Loh et al., 2010). In recent years, the functionalized GO has been exploited to fabricate biosensors for drug delivery (Liu et al., 2008; Zhang et al., 2010a), bioimaging in living cells (Wang et al., 2010; Sun et al., 2008), the detection of cancer cell (Tao et al., 2013), glucose (Song et al., 2010), DNA (Liu et al., 2010a; Gao et al., 2014), enzyme (Zhang et al., 2010b), protein (Liu et al., 2010b), peptides (Han et al., 2010), and cellulose and lignin (Yang et al., 2010).

We report an ultrasensitive fiber optic biosensor utilizing GO layer coated on fiber grating device as the linking interface for label-free immunoassay detection. In this work, for the first time, we propose a new GO deposition method based on the chemical-bonding in conjunction with physical-adsorption. As the schematic illustration in Fig. 1, the dLPG coupled the light from fiber core to cladding serving as an optical transducer. The GO layer was coated over the dLPG surface and then immobilized by bioreceptor IgG leaving the binding sites free for specific anti-IgG recognition. The kinetic binding between antibody and antigen altered the dLPG transmission spectrum and was monitored in real-time as a change in local refractive index (RI), thereby eliminating the need of analyte labeling. The GO-dLPG based biosensor with extremely enhanced sensitivity can detect the optical signal change due to biochemical, bioaffinity, immunogenic interactions occurring within the evanescent field.

2. Materials and methods

2.1. Materials

The aqueous dispersion of graphene oxide (2 mg/mL), Sodium hydroxide (NaOH), (3-Aminopropyl)triethoxysilane (APTES), N-(3-Dimethylaminopropyl)-N'-ethylcarbodiimide hydrochloride (EDC), N-Hydroxysuccinimide (NHS), Bovine serum albumin (BSA), Rabbit IgG, Goat Anti-Rabbit IgG and phosphate buffered saline (1×PBS, pH 7.4) were purchased from Sigma-Aldrich (United Kingdom). Hydrochloric acid (HCl), methanol, ethanol, acetone, and deionized (DI) water were purchased from Thermo Fisher Scientific Inc. (United Kingdom).

All chemical and biochemical reagents were of analytical grade and were used as received without further purification. All aqueous solutions were prepared with DI water.

The silica single-mode fiber (SMF-28, cladding diameter 125 μm) was purchased from Corning.

2.2. Fabrication of dual-peak long period grating

The dLPG with period of 162 μm and length of 30 mm was inscribed in a hydrogenated single-mode fiber by a CW frequency-doubled Ar laser at 244 nm wavelength. The point-by-point method over multiple iterations was employed to achieve the dual-peak feature. After UV fabrication, the dLPG was annealed at 80 $^{\circ}\text{C}$ for 48 h to remove the residual hydrogen and to stabilize the optical properties.

2.3. Functionalization of GO-dLPG sensor

Deposition of graphene and its derivatives on fiber surface could enhance the performance of optical fiber devices (Wu et al., 2014; Sridevi et al., 2016). However, the lack of efficient transfer techniques limited the usage of graphene and GO for fiber device with cylindrical shape and small diameter.

In this work, we develop the GO deposition on the optical fiber surface by APTES as cross-linking agent followed by physical adsorption. Immobilization of biomolecule plays a crucial role in generating a biosensor with high sensitivity, stability and durability. The device surface must be modified to introduce functional groups, which can immobilize bioreceptor on the surface serving as an analytical platform for biological events.

2.3.1 Surface silanization and GO deposition

Fig. 2 plots the schematic scheme of the functionalization of a GO-dLPG as a label-free biosensor. The section of silica fiber over the dLPG region was cleaned by the use of acetone solution for 30 min to remove the organic contaminant, rinsed with DI water thoroughly and dried. Then the fiber device was immersed in 1.0 M NaOH solution for 1 h at room temperature to enrich the number of silanol (Si-OH) groups on the surface and washed

with ethanol and DI water for three times respectively (Fig. 2a).

For the silanization, the alkaline-treated fiber was firstly incubated into a freshly-prepared 5% (v/v) APTES ethanol solution for 1 h, which mainly reacted with hydroxyl groups to form Si-O-Si bonding, followed by washing with ethanol to remove unbound monomers and baked in an oven at 70 $^{\circ}\text{C}$ for 30 min to enhance the stability of APTES monolayer (Fig. 2b).

After APTES silanization, the fiber was immersed in 80 $\mu\text{g}/\text{mL}$ GO aqueous solution contained in a custom-made mini-bath, which was placed on a hot plate at 42 $^{\circ}\text{C}$ for 3 h. The epoxy group of GO reacted with amino group of APTES-silanized fiber (Wang et al., 2008) while the aqueous solution was being slowly evaporated and GO nanosheets were gradually and physically adsorbed on the fiber surface. After this procedure, the GO-coated fiber was soaked into DI water for 30 min to remove the unbound GO sheets, followed by placing it into an oven at 70 $^{\circ}\text{C}$ for 1 h to consolidate the GO layer (Fig. 2c).

2.3.2 Biofunctionalization of GO surface

Immobilization of biomolecules on device surface is an important step in the biosensor development. The covalent immobilization of IgG on GO-dLPG surface might lead to improper orientation by masking antigen-binding sites. This shortcoming can be circumvented by using heterobifunctional cross-linkers of EDC/NHS combination (Dixit et al., 2011).

The GO-coated dLPG was immersed into a mixture of 20 mM EDC and 40 mM NHS in 0.01 M PBS buffer for 1 h. Subsequently, the GO surface was immobilized by IgG through sinking the GO-dLPG into a solution of rabbit IgG with a concentration of 1 mg/mL for 2 h. The large 2D aromatic surface of GO made it ideal for biomolecules binding. GO reacted with EDC to yield a stable active ester in the presence of NHS while the ester reacted with the amine group of IgG to form a covalent immobilization leaving the binding sites free for anti-IgG recognition (Fig. 2d).

The non-bound IgG was washed away by 1 \times PBS buffer solution which was adjusted to a pH of 7.4. The unreacted sites on GO surface were passivated by BSA, the IgG-immobilized GO-dLPG was immersed into 1 % BSA solution for 30 min to

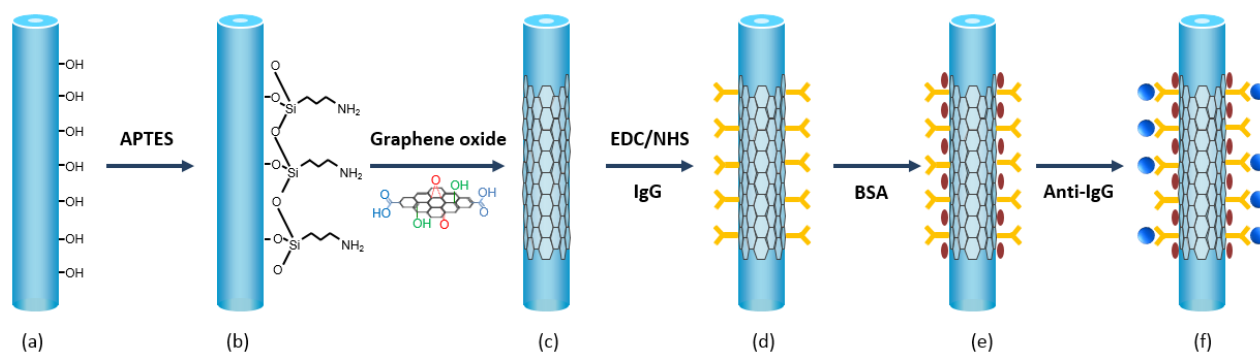


Fig. 2. Schematic illustration of fiber optic biosensor based on GO-coated dLPG: (a) dLPG silica fiber surface with alkaline treatment, (b) Silanization by APTES, (c) GO deposition, (d) IgG immobilization via EDC/NHS, (e) Passivation of unreacted sites by BSA blocking solution, (f) Binding interaction between probe bioreceptor (IgG) and target analyte (anti-IgG).

block the remaining activated carboxylic group and to prevent non-specific adsorption onto GO surface (Fig. 2e). Here, the IgG-bound GO-dLPG was ready as a biosensor for the detection of target anti-IgG (Fig. 2f).

2.4. Measurement system and data analysis

In the interrogation system, broadband light source (BBS: Agilent HP83437A, Agilent Technologies Inc.) was used along with an optical spectrum analyzer (OSA, Agilent HP86142A, Agilent Technologies Inc.). The OSA was connected to a computer and the optical spectra were captured by a customized program. Data analysis was performed using the customized program which automatically defined resonance wavelengths using the centroid calculation method.

All biochemical experiments were performed in a fume cupboard. All procedures were conducted at a controlled room temperature of 22.0 ± 0.1 °C unless specified otherwise. **The long period fiber grating was illuminated with the light from the broadband source and the transmission spectrum was monitored in real-time by using the OSA.** To minimize the bend cross-sensitivity, the fiber grating region was placed straight in a custom-made V-groove container on a Teflon plate and all the chemicals and solvents were added and withdrawn by careful pipetting.

3. Results and discussion

3.1. Surface morphological characterization

The surface morphology of GO coating was characterized by Raman spectroscopy, Atomic force microscopy (AFM), and Scanning electron microscope (SEM).

GO-coated fiber was initially examined by using optical microscope (Fig. 3a). There is a clear boundary between bare and GO-coated sections demonstrating a successful overlay deposition on fiber surface.

Raman spectroscopy is one of the most powerful tools used to characterize the properties of carbon-based materials. Renishaw Raman Microscope 1000 (with 632.8 nm light) was used to characterize GO coating. **The Raman spectrum of GO material has been depicted in Fig. S1.** In comparison with bare fiber, the Raman spectrum of GO-coated fiber presented as red curve in Fig. 3b consists of three prominent peaks assigned to the first order D (1335 cm^{-1}) and G modes (1599 cm^{-1}) and the second order 2D mode ($\sim 2682\text{ cm}^{-1}$) indicating the presence of GO. The D mode was assigned to local defect and disorder of GO caused by attachment of hydroxyl and epoxide groups on the carbon basal plane and edges. The G mode was due to the first order scattering of the E_{2g} plane of sp^2 carbon atoms (Li et al., 2009).

Thickness of the GO layer depended on the conditions of deposition and was identified by AFM (Veeco Instruments Inc., di Dimension 3100). Fig. 3c is AFM tapping mode topographic image of GO layer coated on fiber surface with a thickness of

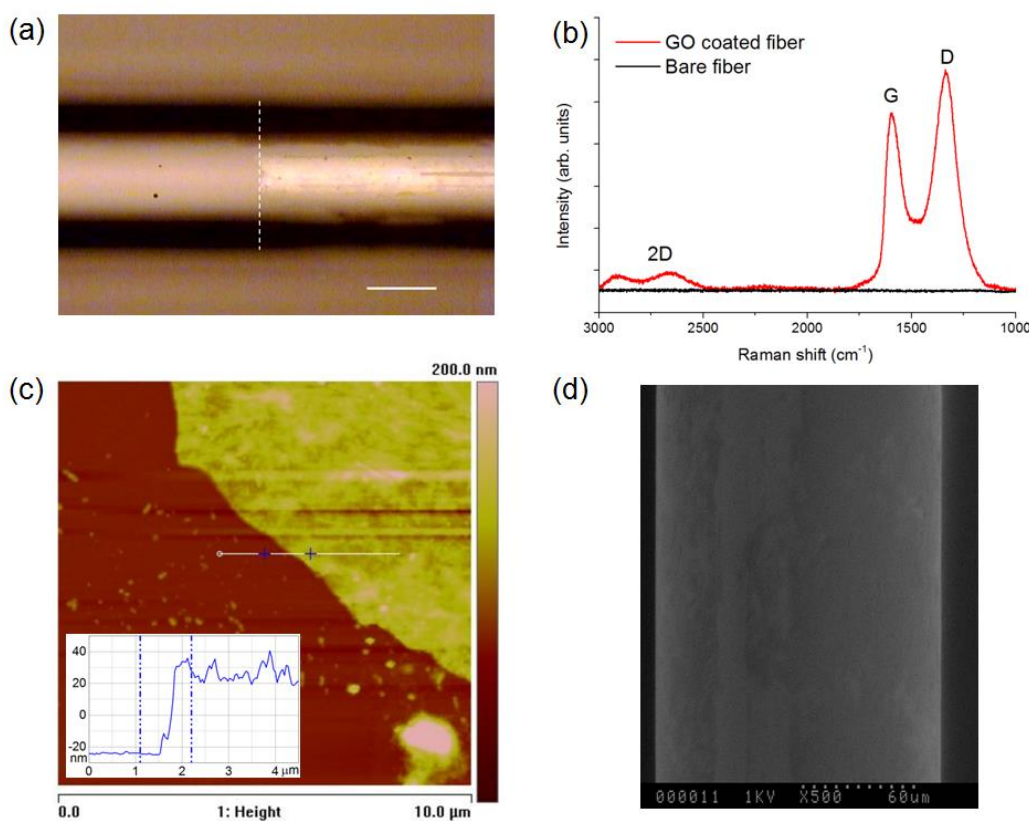


Fig. 3. (a) Optical image of GO-coated fiber (dotted line: GO boundary, scale bar: 50 μ m), (b) Raman spectra, (c) Atomic Force Micrograph of GO step boundary (inset: height profile of GO overlay), (d) Scanning Electron Micrograph of GO overlay on fiber surface.

49.22 nm (inset in Fig. 3c) and a root-mean-squared surface roughness of 2.19 ± 0.01 nm.

The surface coverage of GO was imaged by SEM (Hitachi, S-520) operated at 1 KV (Fig. 3d). The GO layer was **slightly wrinkled-but** quite homogeneous over the entire cylindrical surface of the fiber.

3.2 Characteristics of sensitivity in refractive index

An LPG couples the light from the fundamental core mode to the co-propagating cladding modes yielding distinct attenuation bands in the transmission spectrum at discrete resonant wavelengths satisfying the phase-matching condition (Vengsarkar et al., 1996):

$$\lambda_{res} = (n_{co}^{eff} - n_{cl,m}^{eff})\Lambda \quad (1)$$

where n_{co}^{eff} and $n_{cl,m}^{eff}$ are the effective refractive indices of core and m th cladding mode, Λ is the grating period. Due to the parabolic property of the group index of the higher cladding modes, there is a set of dispersion turning points (DTPs) which exists on the phase-matching curves (She et al., 2002; Chen et al., 2005). For a 162 μ m-period dLPG used in this work, the light coupling from core mode to the 12th order cladding mode led to two attenuation peaks LP_{012}^{blue} at 1340 nm and LP_{012}^{red} at 1465 nm (measured in DI water, Fig. 4a) in the transmission spectrum with respect to the same conjugate cladding mode

(LP_{012}). LPG with such dual peaks featuring wavelength shift of opposite sign to the same external RI perturbation was defined as dual-peak LPG (dLPG).

The RI sensitivities of bare and GO-coated dLPGs were investigated and compared by immersing the fiber sensors in a set of aqueous sucrose solutions. The solutions with concentrations of 0, 10, 20, 30, 35, 40, 45, 50, 55 and 60 % were prepared with measured RIs of 1.3326, 1.3471, 1.3625, 1.3820, 1.3917, 1.4004, 1.4101, 1.4218, 1.4300 and 1.4413, respectively. The fiber sensor was placed in a V groove while the sucrose solution samples were added by careful pipetting to cover the entire grating region. After each measurement, both fiber sensor and V groove were rinsed with methanol and DI water thoroughly. Fig. 4a and Fig. 4b plot the evolution of transmission spectrum against different sucrose concentrations for bare dLPG and GO-dLPG, respectively. Dual peaks move to opposite directions when SRI increases, in which the red-peak LP_{012}^{red} moves to the long wavelength while the blue-peak LP_{012}^{blue} shows a blue shift. In contrast, the LP_{011} peak only shows a slight blue shift.

As it can be seen in Fig. 4b, the intensities of GO-dLPG dual-peaks are significantly reduced when the SRI increases, this is consistent with the previous investigation (Villar et al., 2005; Cusano et al., 2005). For a long period grating coated with high RI and thin layer, the cladding guided modes are partially radiated to the overlay behaving as leaky modes. The

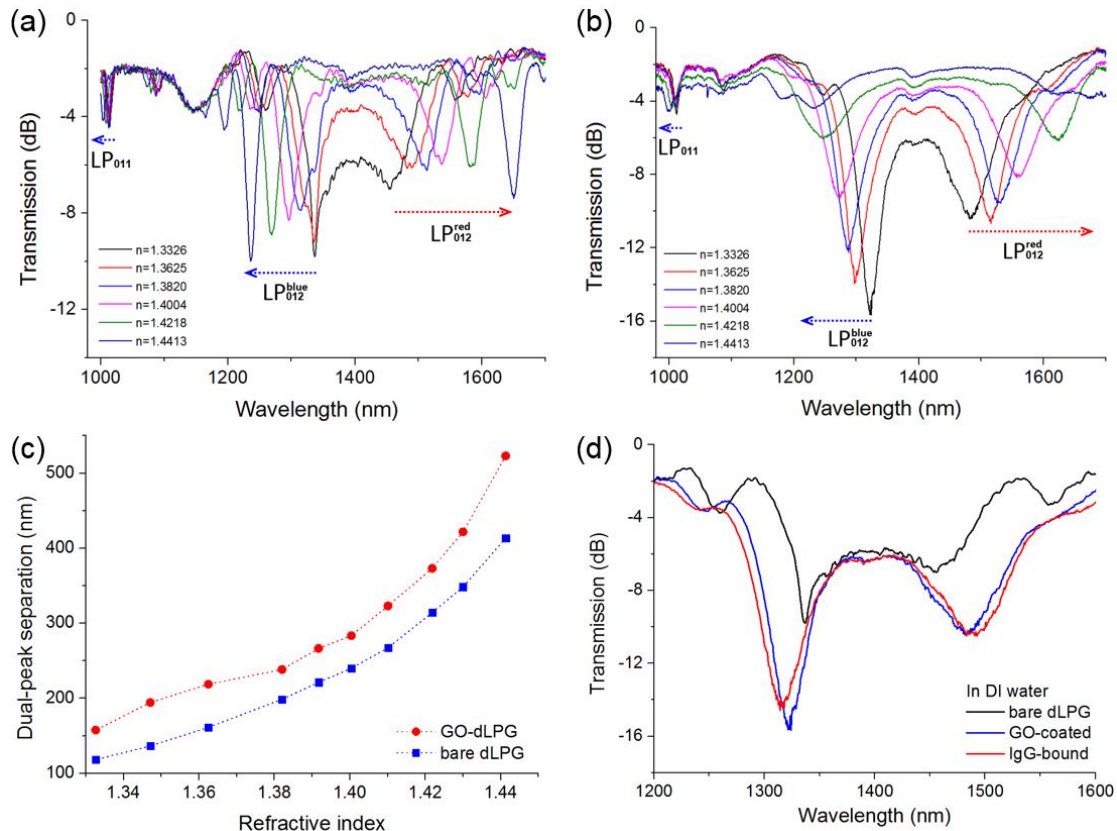


Fig. 4. Transmission spectra of bare dLPG (a) and GO-dLPG (b) measured in different sucrose concentrations, (c) Dual-peak wavelength separation against SRI, (d) Spectra evolution of non-coated, GO-coated, and IgG-immobilized dLPG.

coupling coefficient between optical modes is a function of the SRI. The increasing SRI reduces the overlap integral between core and cladding modes, hence the decreasing of resonant intensity (Erdogan, 1997; Tan et al., 2014). When the SRI approaches that of cladding, the core mode will be coupled to the broadband radiation mode with no distinct attenuation bands.

Fig. 4c plots the dependence of dual-peak separation against the change of SRI, demonstrating a non-linear relationship. The red symbols representing GO-dLPG show the RI sensitivities of 2538 nm/RIU and 8956 nm/RIU for low (1.333-1.347) and high (1.430-1.441) RI regions respectively, while the blue symbols of non-coated dLPG give sensitivities of 1255 nm/RIU and 5761 nm/RIU for the corresponding RI regions. The RI sensing mechanism relies on the sensitivity of long period grating's attenuation bands to the properties of overlay material, such as refractive index and the thickness. With a proper GO thickness of 49.2 nm, the RI sensitivities of GO-dLPG have been improved 200% and 155% those of non-coated dLPG for low and high RI regions, respectively. The GO deposition enhances the light-matter interaction between cladding and surrounding medium leading to the increase of RI sensitivity.

The influence optical responses of GO deposition and IgG immobilization were determined by monitoring the transmission spectra. Fig. 4d depicts the transmission spectra captured in DI water before and after GO deposition, and after IgG immobilization. As shown in the figure, both the separation and the intensity of dual peaks have been increased with respect to the GO deposition and IgG immobilization procedures. The GO deposition induces the wavelength separation from 120 nm to 155 nm while the IgG immobilization expands it to 165 nm.

It was reported that the rapid variation of the gradient of the phase matching curves near the DTP caused the sensitivity of the particular resonant bands to environmental perturbation to be determined by its proximity to its DTP (She et al., 2002). It should be noted that the GO deposition has tuned dual peaks away from its DTP (Fig. 4d) which might sacrifice the bulk RI sensitivity of dLPG device. However, a small weakness did not

cover the merits of GO as a coating material. The RI sensitivity of dLPG coated by GO with a proper thickness of 49.2 nm was increased over 155%. In particular, the presence of GO enhanced the RI sensitivity by a factor of 2 in low RI region (1.333-1.347), the range in which bioassays and biological events were usually carried out. Moreover, GO functionalized dLPG demonstrate remarkable sensitivity in biosensing which will be discussed in next section.

3.3. Evaluation of antibody-antigen kinetic binding interaction

The advantage of fiber grating based biosensor was that signal response was obtained continuously in the concentration-dependent manner in which signal was monitored in real-time. The feasibility of GO-dLPG immunosensor was performed by using rabbit IgG immobilized GO-dLPG to detect the kinetic binding with goat anti-rabbit IgG.

Four consecutive processes for different goat anti-rabbit IgG concentrations of 1, 10, 50, and 100 $\mu\text{g/mL}$ were plotted in Fig. 5. For each process with the specific anti-IgG concentration, the LP_{012}^{red} peak of GO-dLPG was monitored *in situ* throughout whole process. As shown in Fig. 5, each process was performed in three stages: i) Prewashing the rabbit IgG-immobilized GO-dLPG with PBS buffer (1 \times PBS, pH 7.4) for 5 min, providing a stable baseline over which the peak signal was monitored (Fig. S2(a)). ii) Kinetic binding stage when the IgG-immobilized sensor was immersed in goat anti-rabbit IgG solution. The first 3 min is a rapid reaction process during which the grating peak moved to the long wavelength dramatically (Fig. S2(b)), followed by a 27 min steady process when the signal was moving gradually and achieving the saturation finally. iii) A subsequent rinsing with PBS buffer thoroughly to remove unbound anti-IgG prior to the next measurement for another anti-IgG concentration. During four antibody-antigen binding processes, the grating peak wavelength shifts as absolute change in refractive index after deducting the baseline signal in PBS were 1470, 1730, 2415, and 1960 pm for anti-IgG concentrations of 1, 10, 50, and 100 $\mu\text{g/mL}$, respectively. The

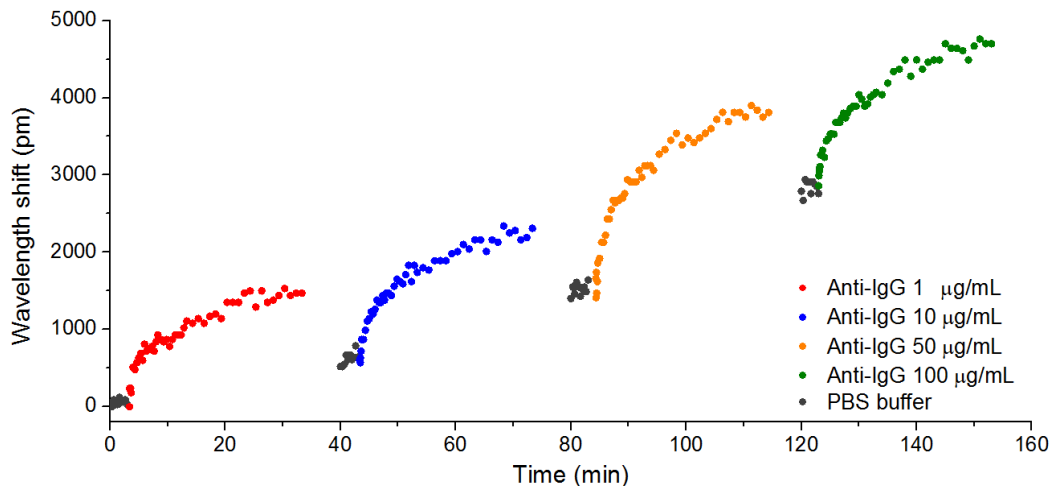


Fig. 5. Wavelength shift against time during IgG and Anti-IgG binding interaction processes.

slight decrease in the 4th binding process (e.g. 100 $\mu\text{g/mL}$ anti-IgG) indicated the gradual depletion of binding sites on sensor surface. The wavelength shift corresponding to the total amount of antibody-antigen binding was 4735 pm. **The wavelength shift of LP_{012}^{red} peak as a function of the concentration of each anti-IgG solution has been plotted in Fig. 6.** The red line provides the best logistic curve fitting of the experimental data, whereas the dashed line represents the wavelength change three times the standard deviation of the blank measurement in PBS buffer. For this GO-dLPG based biosensor, the limit of detection (LOD) of 7 ng/mL is achieved, which is defined as three times the standard deviation of the blank measurement (Fig. 6). This LOD is 10-fold better than non-coated dLPG based biosensor (Chiavaioli et al., 2014) and 100-fold lower than LPG-based immunosensor (DeLisa et al., 2000).

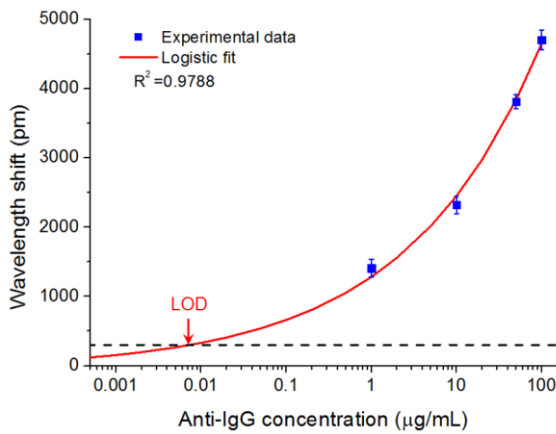


Fig. 6. Dependence of wavelength shift against anti-IgG concentrations. **The red line is the best logistic fitting curve.**

The mechanism of biosensing is that the bioaffinity binding changes local refractive index at the GO-analyte interface, where the evanescent light penetrates, and induces an optical signal change. The sensitivity of the GO-dLPG biosensor can be defined as the ratio of the change in optical signal to the changes in the measurement quantity. The biosensor sensitivity is given by

$$S = \frac{\Delta\lambda}{\Delta C} = \frac{\Delta\lambda}{\Delta n} \frac{\Delta n}{\Delta C} = S_{RI} E \quad (2)$$

where $\Delta\lambda$ is the wavelength shift, ΔC is the change of the analyte concentration, and Δn is the corresponding refractive index change. **The affinity binding between antibody and antigen alters the local analyte concentration (ΔC), increasing the local refractive index (Δn) at device and surrounding-media interface, hence induces the optical signal change with the corresponding wavelength shift ($\Delta\lambda$).**

Therefore, the biosensor sensitivity comprises of two parts: sensitivity to refractive index change S_{RI} and the binding efficiency E . The efficiency depends on the property of sensor surface, the number of binding sites, and the type of bio-analyte. Due to the inherently high surface-to-volume ratio, enriched functional groups and excellent optical and biochemical

properties, the usage of GO as a bio-interface linking layer provides large amount of binding sites, high immobilization density, great biocompatibility and stability, and strong interference of optical waves. The GO-dLPG exhibits not only the enhancement of RI sensitivity but also the extremely higher efficiency, ensuring remarkable performance for biosensing applications with the advantages of label-free, real-time, ultrahigh sensitivity and competitive limit of detection.

3.4. Reusability of GO-dLPG biosensor

For the practical applications, the reusability is an important and must-have function. To this end, we have assessed the reusability by regenerating the biosensor surface activity with HCl treatment.

The above IgG/anti-IgG bound sensor was submerged into 0.01 M HCl solution for 10 min at room temperature, which formed a low pH environment (pH 2.0) and broke the bonds between IgG and anti-IgG, then rinsed with PBS buffer and dried. After stripping off the anti-IgG, its reusability was confirmed by detecting the binding interaction in 1 $\mu\text{g/mL}$ goat anti-rabbit IgG for multiple times (Fig. S3).

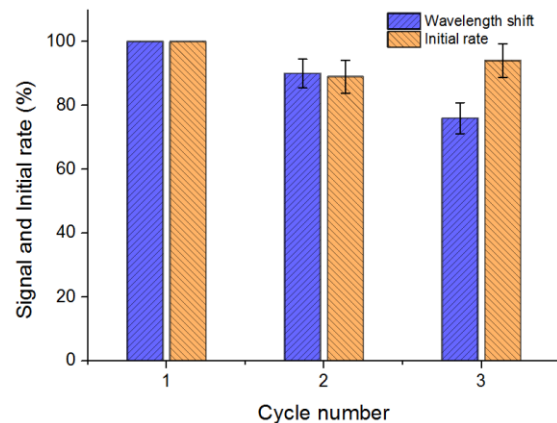


Fig. 7. Reusability of GO-dLPG demonstrated by percentages of peak signal (blue bar) and initial binding rate (orange bar) in comparison with three cycles.

Fig. 7 presents the comparison results for three cycles with the percentages of peak signal and initial binding rate. The maximum peak signal as the absolute change in RI after reducing the baseline signal in PBS prewashing stage retained 90% and 76% after 2nd and 3rd cycle, respectively. Likewise, the initial binding rate calculated with the data over the first 1 min of binding interaction kept greater than 89% and 94% after 2nd and 3rd cycle, respectively. These results confirmed that the GO-dLPG biosensor was possible to measure the antibody-antigen binding for multiple times.

4. Conclusion

We propose a label-free biosensor based on GO-coated dLPG to detect the bioaffinity between antibody and antigen in real-time. A new GO deposition technique based on the

chemical-bonding in conjunction with physical-adsorption has been developed to achieve the desirable stability, repeatability and durability of GO layer on fiber surface. With GO deposition, the RI sensitivity of dLPG has been enhanced by 200% and 155% in low RI (1.333-1.347) and high RI (1.430-1.441) region, respectively. The GO-dLPG has been biofunctionalized with IgG to detect a quantifiable optical signal corresponding to the refractive index change of the analyte in which the IgG and anti-IgG binding interaction occurred. The achievable limit of detection is 7 ng/mL, which is 10-fold better than non-coated dLPG biosensor and 100-fold greater than LPG-based immunosensor. Moreover, the reusability has been facilitated by stripping off bound anti-IgG treatment. The proposed GO-dLPG biosensor provides a remarkable bioanalytical platform for biosensing with the advantages of label-free, real-time monitoring, ultrahigh sensitivity and multiple usability.

Acknowledgements

The authors are grateful for the support from the projects of EU FP7 PIRSES-2013- 612267 and the Sêr Cymru NRN097.

Appendix A. Supplementary material

Supplementary data associated with this article can be found in the attached file.

References

- Ablert, J., Shao, L.Y., Caucheteur, C., 2013. *Laser and Photonics Reviews* 7(1), 83-108.
- Bao, Q., Zhang, H., Wang, Y., Ni, Z.H., Yan, Y.L., Shen, Z.X., Loh, K.P., Tang, D.Y., 2009. *Adv. Funct. Mater.* 19 (19), 3077-3083.
- Bao, Q., Zhang, H., Yang, J.X., Wang, S., Tang, D.Y., Jose, R., Ramakrishna, S., Lim, C.T., Loh, K.P., 2010. *Adv. Funct. Mater.* 20, 782-791.
- Bonaccorso, F., Sun, Z., Hasan, T., Ferrari, A. C., 2010. *Nature Photon.* 4, 611-622.
- Brzozowska, E., Smietana, M., Koba, M., Gorska, S., Pawlik, K., Gaman, A., Bock, W.J., 2015. *Biosens. Bioelectron.* 67, 93-99.
- Canning, J., 2009. *J of Sensors* 2009, 871580, 17 pages.
- Chen, D., Feng, H., Li, J., 2012. *Chem. Rev.* 112 (11), 6027-6053.
- Chen, X., Zhang, L., Zhou, K., Davies, E., Sugden, K., Bennion, I., Hughes, M., Hine, A., 2007. *Opt. Lett.* 32, 2541-2543.
- Chen, X., Zhou, K., Zhang, L., Bennion, I., 2005. *Appl. Opt.* 44, 178-182.
- Chiavaioli, F., Biswas, P., Trono, C., Bandyopadhyay, S., Giannetti, A., Tombelli, S., Basumallick, N., Dasgupta, K., Baldini, F., 2014. *Biosens Bioelectron.* 60, 305-310.
- Cusano, A., Consales, M., Crescitelli, A., Ricciardi, A., (Eds.) 2014. Springer.
- Cusano, A., Iadicicco, A., Pilla, P., Contessa L., Campopiano, S., Cutolo, A., Giordano, M., 2006. *Opt. Express* 14, 19-34.
- Deep, A., Tiwari, U., Kumar, P., Mishra, V., Jain, S., Singh, N., Kapur, P., Bharadwaj, L., 2012. *Biosens Bioelectron.* 33, 190-195.
- DeLisa, M.P., Zhang, Z., Shiloach, M., Pilevar, S., Davis, C.C., Sirkis, J.S., Bentley, W.E., 2000. *Anal. Chem.* 72, 2895-2900.
- Ding, J., Zhang, A., Shao, L-Y., Yan, J-H., He, S., 2005. *IEEE Photon. Technol. Lett.* 17, 1247-1249.
- Dixit, C.K., Vashist, S.K., MacCraith, B.D., O’Kennedy, R., 2011. *Nat. Protoc.* 6, 439-445.
- Dreyer, D. R., Park, S., Bielawski, C. W., Ruoff, R. S., 2010. *Chem. Soc. Rev.* 39, 228-240.
- Erdogan, T., 1997. *J. Opt. Soc. Am. A* 14, 1760-1773.
- Estevez, M., Otte, M. A., Sepulveda, B., Lechuga, L. M., 2014. *Analytica Chimica Acta* Vol. 806, 55-73.
- Fan, X. and White, I.M., 2011. *Nature Photonics*, 5, 591-597.
- Gao, L., Lian, C., Zhou, Y., Yan, L., Li, Q., Zhang, C., Chen, L., Chen, K., 2014. *Biosens. Bioelectron.* 60, 22-29.
- Geim, A.K., 2009. *Science* 324, 1530-1534.
- Han, T.H., Lee, W.J., Lee, D.H., Kim, J.E., Choi, E.Y., Kim, S.O., 2010. *Adv. Mater.* 22 (18), 2060-2064.
- He, Z., Tian, F., Zhu, Y., Lavlinskaia, N., Du, H. 2011. *Biosens Bioelectron.* 26, 4774-4778.
- James, S. W. and Tatam, R. P., 2003. *Meas. Sci. Technol.* 14, R49-R61.
- Jang, H.S., Park, K.N., Kim, J.P., Sim, S.J., Kwon, O.J., Han, Y.G., Lee, K.S., 2009. *Opt Express.* 17, 3855-3860.
- Lepinay, S., Staff, A., Ianoul, A., Albert, J., 2014. *Biosens. Bioelectron.* 52, 337-344.
- Li, X., Cai, W., An, J., Kim, S., Nah, J., Yang, D., Piner, R., Velamakanni, A., Jung, I., Tutuc, E., Banerjee, S.K., Colombo, L., Ruoff, R.S., 2009. *Science* 324 (5932), 1312-1314.
- Liu, J.B., Li, Y.L., Li, Y.M., Li, J.H., Deng, Z.X., 2010a. *J. Mater. Chem.* 20, 900-906.
- Liu, J.B., Fu, S.H., Yuan, B., Li, Y.L. Deng, Z.X., 2010b. *J. Am. Chem. Soc.* 132 (21), 7279-7281.
- Liu, Z., Robinson, J.T., Sun, X., Dai, H., 2008. *J. Am. Chem. Soc.* 130, 10876-10877.
- Loh, K.P., Bao, Q., Eda, G., Chhowalla, M., 2010. *Nat. Chem.* 2, 1015-1024.
- Luo, B., Yan, Z., Sun, Z., Li, J., Zhang, L., 2014. *Opt. Express* 22, 30571-30578.
- Marks, R.S., Lowe, C. R., Cullen, D. C., Weetall, H. H., Karube, I., 2007. *Handbook of Biosensors and Biochips*. Wiley, Weinheim.
- Marques, L., Hernandez, F.U., James, S.W., Morgan, S.P., Clark, M., Tatam, R.P., Korposh, S., 2016. *Biosens Bioelectron.* 75, 222-231.
- Morales-Narváez, E. and Merkoç, A., 2012. *Adv. Mater.* 24 (25), 3298-3308.
- Novoselov, K.S., Geim, A.K., Morozov, S.V., Jiang, D., Zhang, Y., Dubonos, S.V., Grigorieva, I.V., Firsov, A.A., 2004. *Science* 306 (5696), 666-669.
- Pilla, P., Trono, C., Baldini, F., Chiavaioli, F., Giordano, M., Cusano, A., 2012. *Opt. Lett.* 37, 4152-4154.
- Shevchenko, Y., Camci-Unal, G., Cuttica, D., Dokmeci, M., Albert, J., Khademhosseini, A., 2014. *Biosens Bioelectron.* 56, 359-367.
- Shu, X., Zhang, L., Bennion, I., 2002. *J. Lightwave Technol.* 20, 255-266.
- Song, Y., Qu, K., Zhao, C., Ren, J., Qu, X., 2010. *Adv. Mater.* 22, 2206-2210.
- Sridevi, S., Vasu, K. S., Asokan, S., Sood, A. K., 2016. *Opt. Lett.* 41, 2604-2607.
- Sun, X.M., Liu, Z., Welsher, K., Robinson, J.T., Goodwin, A., Zaric, S., Dai, H., 2008. *Nano Res.* 1, 203-212.
- Tao, Y., Lin, Y., Huang, Z., Ren, J., Qu, X., 2013. *Adv. Mater.* 25, 2594-2599.
- Tan, Y.C., Ji, W.B., Mamidala, V., Chow, K.K., Tjin, S.C., 2014. *Sens. Actuators B* 196, 260-264.
- Vengsarkar, A., Lemaire, P., Judkins, J., Bhatia, V., Erdogan, T., Sipe, J., 1996. *J. Lightwave Technol.* 14, 58-64.
- Villar, I.D., Matias, I. R., Arregui, F. J., Lalanne, P., 2005. *Opt. Express* 13, 56-69.

- Voisin, V., Pilate, J., Damman, P., Mégret, P., Caucheteur, C., 2014. *Biosens Bioelectron.* 51, 249-254.
- Wang, S., Chia, P.-J., Chua, L.-L., Zhao, L.-H., Png, R.-Q., Sivaramakrishnan, S., Zhou, M., Goh, R. G.-S, Friend, R. H., Wee, T.-S., Ho, P. K.-H., 2008. *Adv. Mater.* 20, 3440-3446.
- Wang, Y.; Li, Z.; Wang, J.; Li, J.; Lin, Y., 2011. *Trends Biotechnol.* 29 (5), 205-212.
- Wang, Y., Li, Z., Hu, D., Lin, C.T., Li, J., Lin, Y., 2010. *J. Am. Chem. Soc.* 132, 9274-9276.
- Wang, X.D., Wolfbeis, O.S., *Anal Chem.* 2013. 85, 487-508.
- Wu, Y., Yao, B., Zhang, A., Rao, Y., Wang, Z., Cheng, Y., Gong, Y., Zhang, W., Chen, Y., Chiang, K. S., 2014. *Opt. Lett.* 39, 2604-2607.
- Yang, Q., Pan, X., Huang, F., Li, K., 2010. *J. Phys. Chem. C* 114, 3811-3816.
- Yin, M., Wu, C., Shao, L-Y., Chan, W., Zhang, P., Lu, C., Tam, H-Y., 2013. *Analyst* 138, 1988-1994.
- Zhang, L.M., Xia, J., Zhao, Q., Liu, L., Zhang, Z., 2010a. *Small* 6 (4), 537-544.
- Zhang, J.L., Zhang, F., Yang, H.J., Liu, H., Zhang, J.Y., Guo, S.W., 2010b. *Langmuir* 26, 6083-6085.
- Zhao, D., Zhou, K., Chen, X., Zhang, L., Bennion, I., 2004. *Meas. Sci. Technol.* 15, 1647-1650.
- Zhou, K., Simpson, G., Chen, X., Zhang, L., Bennion, I., 2004. *IEEE Photon. Technol. Lett.*, 16, 1549-1551.
- Zhou, L., Mao, H., Wu, C., Tang, L., Wu, Z., Sun, H., Zhang, H., Zhou, H., Jia, C., Jin, Q., Chen, X., Zhao, J., 2017. *Biosens. Bioelectron.* 87 (15), 701-707.